SUPPLEMENT

REVISTA DE Biología Tropical

https://doi.org/10.15517/fqq12565

FragSize: using computer vision models to monitor massive coral fragment growth in a Caribbean coral nursery in the Seaflower Biosphere Reserve

Yanelys Cantillo Villa [1]; https://orcid.org/0009-0000-7745-3540.
Susana Cuellar Uribe [2]; https://orcid.org/0009-0006-4908-9693
Bruce Hoyos Mendoza [1]; https://orcid.org/0009-0000-5307-5629
María Fernanda Maya [1*]; https://orcid.org/0000-0002-7839-026X

1. Blue Indigo Foundation, archipelago of San Andrés and Providencia, Colombia; ycantillovi@unal.edu.co, brucew.hoyosmendoza@gmail.com, mfmaya@blueindigofoundation.org (*Correspondence)
2. Biology Department, University of Los Andes, Bogotá D.C, Colombia; s.cuellaru@uniandes.edu.co

Received 14-I-2026. Corrected 10-VI-2026. Accepted 18-VI-2026.

ABSTRACT

Introduction: Monitoring the growth of coral fragments in restoration nurseries is essential for assessing their performance and the effectiveness of restoration interventions. Two-dimensional methods based on digital photography and ImageJ are commonly used, but their manual nature is time-consuming.

Objectives: The aim of this study was to evaluate and test the performance of FragSizel, this open-source tool uses a computer-vision YOLOv8 segmentation model to automatically estimate the planar surface area of coral fragments from two-dimensional images. The evaluation of the performance of the model focused on assessing the degree of agreement between FragSize measurements and those obtained with traditional manual methods such as ImageJ.

Methods: A YOLOv8 segmentation model was trained using photographs of fragments of *D. labyrinthiformis*, *O. faveolata*, and *M. cavernosa* that were kept an in-situ nursery at Nirvana Reef Garden, San Andrés Island (Colombian Caribbean). Agreement between FragSize and ImageJ measurements was assessed using Bland–Altman analyses. A total of 81 fragments of three species and 15 genotypes were measured across T_0–T_1 intervals ranging from 76 to 175 days.

Results: Bland–Altman analyses showed strong agreement between FragSize and ImageJ, with low levels of bias and relative error in measurements performed at T_0 and T_1 under both calibration methods evaluated.

Conclusions: FragSize proved to be a reproducible tool for the automatic estimation of planar area in coral fragments from 2D images, showing agreement with ImageJ-derived measurements under both calibration strategies evaluated. Its open availability on GitHub facilitates its adoption in coral restoration programs requiring accessible and standardized methods for monitoring coral growth.

Key words: Caribbean; coral restoration; monitoring; computer vision.

RESUMEN

FragSize: uso de modelos de visión artificial para monitorear el crecimiento masivo de fragmentos de coral en un vivero de coral caribeño en la Reserva de la Biosfera Seaflower

Introducción: El monitoreo del crecimiento de fragmentos de coral en guarderías de restauración es fundamental para evaluar su desempeño y la efectividad de las intervenciones de restauración. Si bien los métodos 2D basados en fotografía digital e ImageJ son comunes, su naturaleza manual requiere mucho tiempo.

Objetivos: El propósito de este estudio fue evaluar y probar el desempeño de FragSize, una herramienta de código abierto que utiliza un modelo de segmentación de visión artificial YOLOv8 para estimar automáticamente el área de la superficie plana de fragmentos de coral a partir de imágenes bidimensionales. La evaluación del desempeño del modelo se enfocó en determinar el grado de concordancia entre las estimaciones de área planar generadas por FragSize y aquellas obtenidas mediante métodos tradicionales como ImageJ.

Métodos: Se entrenó un modelo de segmentación YOLOv8 utilizando fotografías de fragmentos de *D. labyrinthiformis*, *O. faveolata* y *M. cavernosa* mantenidos en una guardería *in situ* en Nirvana Reef Garden, isla de San Andrés (Caribe colombiano). La concordancia entre las mediciones obtenidas con FragSize e ImageJ se evaluó mediante análisis de Bland–Altman. En total, se midieron 81 fragmentos pertenecientes a tres especies y 15 genotipos, con intervalos T_0–T_1 entre 76 y 175 días.

Resultados: Los análisis de Bland–Altman mostraron una fuerte concordancia entre FragSize e ImageJ, con bajos niveles de sesgo y error relativo en las mediciones realizadas en T_0 y T_1 para los dos métodos de calibración evaluados.

Conclusiones: FragSize demostró ser una herramienta reproducible para la estimación automática del área planar de fragmentos coralinos a partir de imágenes 2D, mostrando concordancia con las mediciones obtenidas mediante ImageJ bajo ambas estrategias de calibración evaluadas. Su disponibilidad abierta en GitHub facilita su adopción en programas de restauración coralina que requieren métodos accesibles y estandarizados para el monitoreo del crecimiento coralino.

Palabras clave: Caribe; restauración coralina; monitoreo; visión artificial.

INTRODUCTION

Caribbean coral reefs, which provide essential ecosystem services, have experienced a dramatic decline since the late 1970s, with losses estimated between 50 % and 80 %. The loss is being driven by a combination of human impacts, including land-based pollution, coastal development, overfishing, and climate change (Cramer et al., 2020). In the region this decline has been compounded by a marked increase in coral disease incidence, prevalence, and diversity (Green & Bruckner, 2000).

Among the most impactful outbreaks in the Caribbean, we have the White Band Disease epidemics of the 1980s, which caused extensive mortality of the corals *Acropora cervicornis* and *Acropora palmata* (Aronson & Precht, 2001; Gladfelter, 1982), and more recently Stony Coral Tissue Loss Disease (SCTLD). SCLTD has affected more than twenty Caribbean coral species and spread across at least 28 countries and territories, causing severe mortality (Papke et al., 2024). Together, these pressures have profoundly altered the structure and resilience of Caribbean reefs, reducing their capacity for natural recovery even under improved environmental conditions (Roff, 2021).

In response, coral restoration has become a critical strategy to sustain ecosystem services while aiming to mitigate the loss of structural complexity. Although early efforts focused on branching species such as *A. cervicornis* and *A. palmata*, there is now broad recognition of the importance of including slow-growing massive species that contribute to long-term reef stability and are particularly vulnerable to SCTLD (Lirman et al., 2014; Page et al., 2018). Asexual fragmentation, which involves cutting slow-growing massive coral species colonies into small pieces that grow and fuse more rapidly, has emerged as a promising method to scale up restoration. (Forsman et al., 2015; Knapp et al., 2022).

Accurate quantification of coral fragment growth and surface area is essential for selecting resilient genotypes and evaluating restoration success. The suitability of each measurement method depends largely on coral morphology. Traditional two-dimensional approaches based on top-view photography and manual contour tracing in ImageJ remain appropriate for species with relatively flat or hemispherical morphologies, such as many massive corals, where the planar projection closely approximates real surface area (Frias-Torres et al., 2023; Neal et

al., 2015). These methods are valued for their low cost, rapid data collection, and applicability by non-specialized personnel, making them useful in large-scale restoration programs. Low-cost two-dimensional photographic methods, when applied to planar or curved colonies, can still detect meaningful differences in survival and growth, even when implemented by non-expert personnel (Frias-Torres et al., 2023). However, their manual nature limits scalability, and as restoration operations expand, we need to address the challenge of having a higher number of fragments to monitor over time. To address these challenges, we developed *FragSize*, an open-access computer-vision tool designed to automate the estimation of coral fragment planar surface area from two-dimensional images. The software uses a YOLOv8-Seg model to detect and delineate fragments from top-view photographs and incorporates a dual calibration system based on either a visible scale in the image or the known plug diameter. This design enables accurate and reproducible measurements under variable photographic conditions in both *in-situ* and *ex-situ* settings.

In this study, we evaluated the performance of *FragSize* using photographs of three Caribbean massive coral species *Diploria labyrinthiformis*, *Montastraea cavernosa*, and *Orbicella faveolata*, maintained in an *in-situ* nursery at Nirvana Reef Garden (San Andrés Island, Colombia). We compared planar surface area measurements obtained with FragSize to those derived from traditional ImageJ tracings and analyzed growth across two time points and among different genotypes. FragSize produced measurements comparable in accuracy to ImageJ while substantially reducing manual effort, demonstrating its potential as a low-cost approach to improve the efficiency and scalability of coral growth monitoring in restoration programs.

MATERIALS AND METHODS

The study was conducted at the Nirvana Reef Garden *in situ* coral nursery (12°30'33.6" –81°43'53.0) within the Seaflower Biosphere Reserve, San Andrés Island, Colombian Caribbean. The nursery hosts massive coral species commonly used in restoration efforts in the region, including *Diploria labyrinthiformis*, *Orbicella faveolata*, and *Montastraea cavernosa*. Coral fragments of 2 to 6 cm from different genets were generated through asexual fragmentation with a Gryphon diamond bandsaw and attached to either cement or aragonite plugs (3.5–4.3 cm in diameter and 2–3 cm in height) using CorAffix glue. Details of the plug characteristics are detailed in Fig. 1. Each fragment was labeled with a metallic tag for individual identification.

Aragonite plugs are commercially manufactured with standardized dimensions, providing a consistent calibration reference across images. In contrast, cement plugs were manually produced using PVC molds, resulting in greater variability in diameter and height. Despite this variability, cement plugs represented a lower-cost alternative commonly used in restoration settings.

Each fragment was photographed twice. For T_0, photographs were taken either immediately after fragmentation outside the water (for some genotypes), or underwater in the nursery a few days after the fragments had been placed on their plugs when immediate underwater access was not possible. The second photograph (T_1) was taken several months later under underwater nursery conditions. The timing of T_0 image acquisition therefore varied among genotypes due to logistical factors such as diving schedules and personnel availability. In this study, each of the donor colony used to produce fragments was treated as a genotype (assumed to represent a distinct individual), and all fragments derived from it were considered clones. Details on species, genotypes, plug type, and time spent in the nursery are provided in Table 1.

All fragments were produced between March and June 2025 under the Giving Caribbean Corals a Future project, developed within the framework of the global CORDAP initiative.

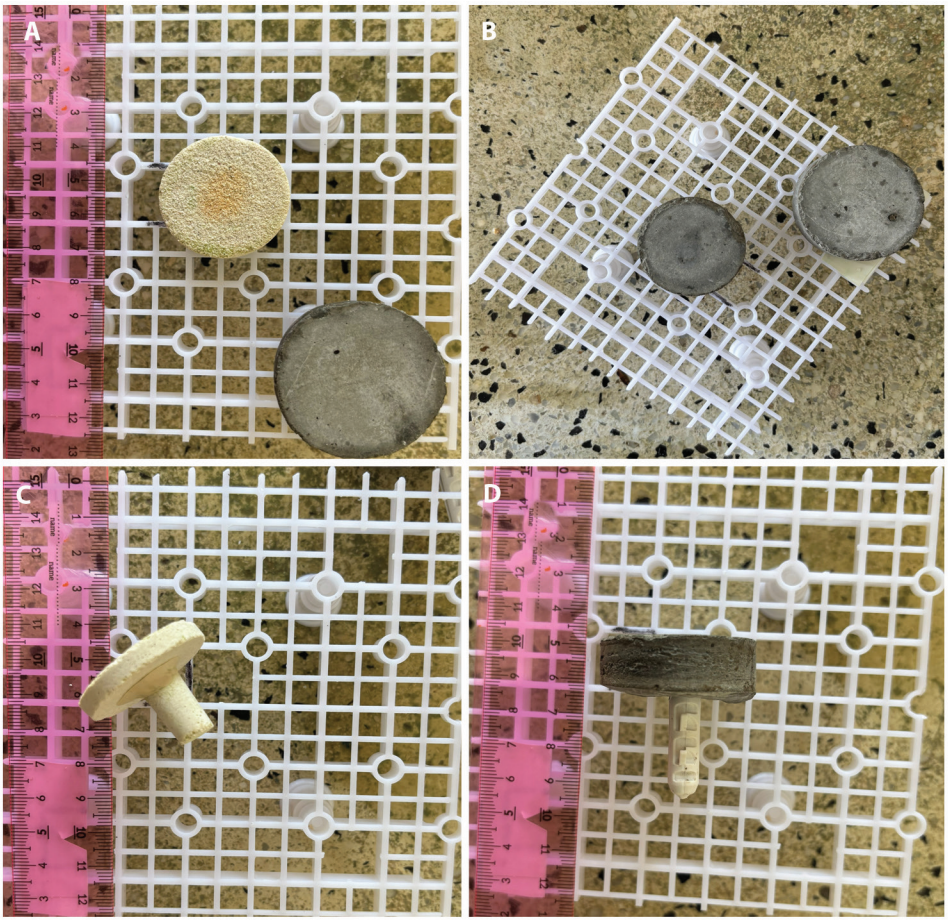

Fig. 1. Characteristics of the experimental plugs used as fragment bases and calibration references. Aragonite plugs (white) and cement plugs (gray) are shown in top **(A–B)** and side **(C–D)** views. Aragonite plugs have a standardized diameter of 3.5 cm, whereas cement plugs exhibit greater variation in size and height.

Species characteristics: The three scleractinian species studied exhibit distinct colony morphologies as described by (Santodomingo et al., 2010). *Diploria labyrinthiformis* forms hemispherical to meandroid colonies, where deep valleys and ridges generate a highly three-dimensional surface that can nevertheless be fragmented into relatively flat, square pieces suitable for planar measurements. *Orbicella faveolata* develops large, dome-shaped colonies with continuous skeletal surfaces and densely packed corallites, typical of massive reef-building forms. *Montastraea cavernosa* grows as plocoid to massive colonies with exserted corallites separated by a well-developed coenosarc, giving the colony a characteristic cavernous appearance with visible gaps between polyps. Asexually, *O. faveolata* and *M. cavernosa* reproduce mainly through extratentacular budding, whereas *D. labyrinthiformis* exhibits intratentacular budding (Santodomingo et al., 2010). Among the studied species, *D. labyrinthiformis* exhibits the most complex three-dimensional morphology, characterized by pronounced ridges and valleys that form deep meandroid structures.

Table 1
Summary of fragment information used for the growth and validation analyses. Each genotype represents a distinct donor colony.

Species	Genotype	Number of fragments	Plug type	Date of production *1	T0	T1	Time in nursery (days)*2
Diploria labyrinthiformis	282	4	aragonite	10/04	29/04	2/09	145
	283	6	aragonite	10/04	29/04	2/09	145
	294	4	cement	14/05	14/05	2/09	110
	295	6	cement	15/05	15/05	2/09	109
	296	6	cement	3/06	3/06	2/09	91
	213	3	cement	17/06	17/06	2/09	76
	211	5	cement	17/06	17/06	2/09	76
Orbicella faveolata	284	7	aragonite	11/03	29/04	2/09	175
	285	5	aragonite	11/03	29/04	2/09	175
	292	9	aragonite	12/03	29/04	2/09	173
	293	9	aragonite	13/03	29/04	2/09	172
Montastraea cavernosa	300	6	aragonite	13/03	29/04	2/09	172
	026	5	cement	8/05	8/05	2/09	116
	027	4	cement	8/05	8/05	2/09	116
	029	2	cement	9/05	9/05	2/09	115

***1.** Date of production" refers to the day when fragments were cut, while T_0 corresponds to the first photograph taken after fragmentation and T_1 to the second photograph obtained after the growth period. / ***2.** "Time in nursery" indicates the duration (in days) that fragments remained in the in-situ coral nursery.

Photographic setting: Each plug of known diameter was photographed either in situ or ex situ using a custom-built photographic station consisting of an acrylic table, a PVC frame, and a fixed vertical camera mount that maintained the camera at a constant distance. The optical axis of the camera lens was aligned perpendicular to the plane of the plug surface to minimize perspective distortion. A 10 cm scale was mounted on the acrylic table as a reference.

Top-view images were captured with a digital Olympus TG-7 camera housed in a Seafrog underwater case, ensuring consistent distance and alignment across monitoring. In some cases, the camera was attached to the photographic station to maintain a fixed height and perpendicular angle. In contrast, in others, it was held manually when attachment was not possible. Nevertheless, camera distance did not vary substantially, since each image was required to include the same portion of the acrylic table showing the complete measuring tape and the fragment's pencil-written label, ensuring a consistent field of view. Some T_0 photographs were captured in air, and T_1 photographs were captured underwater; however, all images contained an in-plane reference (either the visible size scale or a plug of known diameter) used for pixel-to-centimeter calibration. Images were stored in JPEG format at a resolution of 4 000 × 3 000 pixels. The photographic station and its main characteristics are shown in Fig. 2. In some cases, when the Olympus TG-7 was not available, an iPhone 15 camera was used instead.

The photographic station was designed as a portable underwater imaging system to standardize image acquisition across sampling events. The fixed distance between the camera mount and acrylic platform maintained consistent imaging geometry and facilitated scale calibration for planar area estimation.

Model training: A custom deep learning model was developed using Roboflow 3.0 Instance Segmentation (Fast) (Dwyer et al., 2025), based on the YOLOv8-Seg architecture (Jocher et al., 2023). The model was trained to detect and segment individual coral fragments

Fig. 2. Portable photographic station used for standardized imaging of coral fragments underwater. **A.** Lateral view of the PVC frame and mounted digital camera. **B.** Lateral view showing the fixed distance between the camera mount and acrylic platform. **C.** Top view of the acrylic platform with the reference scale used for planar area measurements.

from 2D photographs obtained at the Nirvana Reef Garden coral nursery (San Andrés Island, Colombian Caribbean). The original dataset consisted of 211 annotated images across nine classes, including coral fragments from *Diploria labyrinthiformis*, *Orbicella faveolata*, *Montastraea cavernosa*, *Pseudodiploria strigosa*, and a physical *size scale* reference object.

During preprocessing, all images were resized to 640 × 640 pixels to standardize input dimensions. To enhance model generalization, Roboflow applied automatic data augmentation, expanding the dataset to 1147 total images (1113 for training, 21 for validation, and 13 for testing). Augmentation techniques included random light exposure adjustments between −8 % and +8 %.

Model training was performed in the Roboflow cloud environment using GPU acceleration. The best-performing checkpoint (custom-workflow-instance-segmentation-v19bb/6) was selected for deployment, and the final version (custom-workflow-instance-segmentation-v19bb/7), updated on October 6th, 2025, is available at Roboflow Universe (Dwyer et al., 2025).

According to internal Roboflow metrics, the model achieved a mean Average Precision (mAP@50) of 99.5 %, a Precision of 99.1 %, and a Recall of 99.4 % on the validation set. Class-level performance reached 100 % accuracy for live coral tissue of *Diploria labyrinthiformis*, *Orbicella faveolata*, *Montastraea cavernosa*, and *Pseudodiploria strigosa*, and 95 % accuracy for the *size scale* reference object. Each segmentation output corresponds to a binary mask that delineates the exact pixels belonging to each coral fragment, allowing per-instance isolation and pixel-level measurement of planar surface area. These metrics, while reported within the Roboflow evaluation framework and not necessarily aligned with industry-standard protocols, provide a consistent internal benchmark of segmentation quality. The resulting instance masks and confidence scores were subsequently used to calculate planar surface area and morphological parameters of coral fragments within the *FragSize* analytical workflow.

Application development: FragSize was developed in Python (Python Software Foundation, 2023) as a desktop application integrating the YOLOv8-Seg model (Jocher et al., 2023) for automatic segmentation of coral fragments and a Tkinter-based graphical user interface (GUI) for user interaction. The software enables image loading, mask visualization, and surface area estimation in cm^2 using either a known scale or plug-based calibration. Image processing routines relied on the OpenCV library (Bradski, 2000). The application was built with assistance from OpenAI's Codex and ChatGPT, which supported code generation and documentation refinement throughout development (OpenAI, 2025). FragSize is freely available as an open-source project on GitHub, facilitating transparency, community use, and further improvement.

FragSize integrates automated segmentation and image-based planar area estimation within a graphical user interface designed for coral fragment monitoring. As shown in Fig. 3, the software allows calibration either through a visible reference scale included in the image or

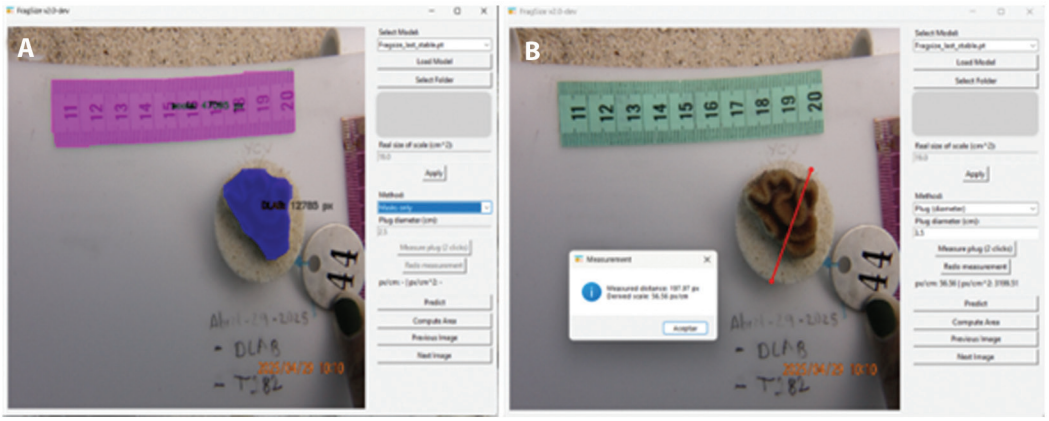

Fig. 3. Workflow and graphical user interface (GUI) of FragSize v2.0. (A) Example of coral fragment segmentation using the YOLOv8-Seg model with calibration based on a visible reference scale. (B) Plug-based calibration mode using the known diameter of the fragment plug. The interface displays binary masks and planar area estimates (cm^2) for each detected fragment.

through the known diameter of the fragment plug, facilitating standardized measurements across different image acquisition conditions.

Model and Application validation: All Statistical analyses were performed in RStudio (RStudio Team, 2022) using R version 4.2.0 (R Core Team, 2022). Measurements from *Diploria labyrinthiformis* were used for validation, as this species exhibits the greatest surface complexity among the studied taxa. The Shapiro–Wilk test was applied to assess data normality, confirming that none of the variables violated the normality assumption. Bartlett's test was used to evaluate the homogeneity of variances among methods, revealing unequal variances for both T_0 and T_1 datasets. Consequently, comparisons among methods were conducted using Welch's one-way ANOVA, which does not assume homogeneity of variances, followed by pairwise Welch *t*-tests (Holm-adjusted) to identify specific differences between measurement methods.

To validate the 2D photogrammetry approaches, coral fragment area measurements obtained with the FragSize application were compared against those obtained with ImageJ. Four calibration approaches were evaluated: (1) FragSize using the size scale visible in the image, (2) FragSize using the known diameter of the aragonite plug, and (3) ImageJ using the plug diameter as a calibration reference 4) ImageJ using the size scale visible in the image. Because manually produced cement plugs are irregular in shape, calibration based on plug diameter was considered more accurate for minimizing potential errors related to the scale plane. Therefore, four datasets were analyzed: ImageJ (scale in image), FragSize (scale in image), FragSize (plug diameter), and ImageJ (plug diameter) for both T_0 and T_1 measurements.

Agreement and interchangeability among methods were further examined through Bland–Altman analyses, in which the difference between paired measurements was plotted against their mean values. Each plot displayed the mean bias and the 95 % limits of agreement (mean ± 2 SD). Statistical significance was set at $p < 0.05$ for all tests.

Growth analysis by species: Fragment growth was assessed by comparing the planar surface area of each fragment between T_0 (initial measurement) and T_1 (follow-up measurement). Analyses were performed separately for each coral species and genotype to capture both interspecific and intraspecific variability in growth performance. Because genotypes

were fragmented on different dates, each one accumulated a different amount of time in the nursery, which needs to be considered when interpreting growth patterns.

The change in planar surface area (ΔArea = $T_1 - T_0$) was used as a proxy for growth. Data normality was assessed using the Shapiro–Wilk test, and homogeneity of variances was evaluated with Levene's test. When both assumptions were met, paired-sample t-tests were used to compare fragment areas between time points; otherwise, the non-parametric Wilcoxon signed-rank test was applied.

For each species genotype combination, the mean and standard deviation (SD) of fragment area were calculated, and results were summarized using boxplots displaying the median, interquartile range, and individual fragment values.

In addition to planar surface measurements, the number of visible polyps was manually counted for *Montastraea cavernosa* fragments at T_0 and T_1 to evaluate biological growth beyond bidimensional expansion. This additional metric was included because growth in *M. cavernosa* is readily observable due to its morphology, where new polyps and increases in polyp size offer a clear indicator of tissue expansion. For *Montastraea cavernosa*, polyp density (polyps·cm^{-2}) was quantified at T_0 and T_1 to assess biological growth beyond planar surface expansion. Polyp density was calculated by dividing the number of visible polyps by the planar area of each fragment at each time point. Normality of paired density differences ($T_1 - T_0$) was evaluated using the Shapiro–Wilk test, after which either paired t-tests or Wilcoxon signed-rank tests were applied to compare polyp density between time points. Descriptive statistics (mean, SD, and range) were computed for each genotype.

RESULTS

Model and application validation: At T_0, area estimates differed significantly among the four measurement methods. Distributions were approximately normal for all methods (Shapiro–Wilk W = 0.94–0.97, $p > 0.08$), but variances were heterogeneous (Bartlett's $K^2 = 14.61$, $p = 0.0022$), so Welch's ANOVA was applied. The analysis revealed a significant effect of method on area ($F_{3,69.5} = 7.14$, $p < 0.001$). Mean ± SD area estimates were 6.13 ± 1.73 cm² for FragSize (scale), 6.54 ± 1.89 cm² for ImageJ (scale), 5.06 ± 1.10 cm² for FragSize (plug), and 5.20 ± 1.13 cm² for ImageJ (plug). Pairwise Welch t-tests with Holm correction showed no difference between the two scale-based methods ($p = 0.73$) nor between the two plug-based methods ($p = 0.73$). In contrast, all comparisons between scale- and plug-based methods were significant ($p \leq 0.036$), indicating that scale calibration systematically produced larger area estimates than plug calibration already at the initial measurement time.

At T_1, the pattern observed at T_0 persisted. Normality was again supported for all methods (W = 0.96–0.98, $p > 0.24$), whereas variances remained heterogeneous (Bartlett's $K^2 = 12.92$, $p = 0.0048$), justifying another Welch's ANOVA. Method had a significant effect on area at T_1 ($F_{3, 69.6} = 6.30$, $p < 0.001$). Scale-based methods yielded the largest areas, with means of 6.09 ± 1.61 cm² for FragSize and 6.24 ± 1.88 cm² for ImageJ, while plug-based methods produced smaller values (4.93 ± 0.99 cm² for FragSize and 5.55 ± 1.32 cm² for ImageJ). As in T_0, pairwise comparisons showed no differences within calibration type (scale-vs-scale: $p = 0.74$; plug-vs-plug: $p = 0.16$), but both scale-based methods differed significantly from both plug-based methods ($p \leq 0.0067$). These results confirm that the upward shift produced by scale calibration is systematic and maintained after months of growth in the nursery. Boxplots comparing area estimates across methods at T_0 and T_1 are shown in Fig. 4.

Scale-based calibration methods produced consistently larger area estimates than plug-based approaches at both T_0 and T_1. However, FragSize and ImageJ showed strong agreement within each calibration strategy. This systematic overestimation by scale-based calibration is likely explained by the fact that the scale is positioned slightly deeper in the image than

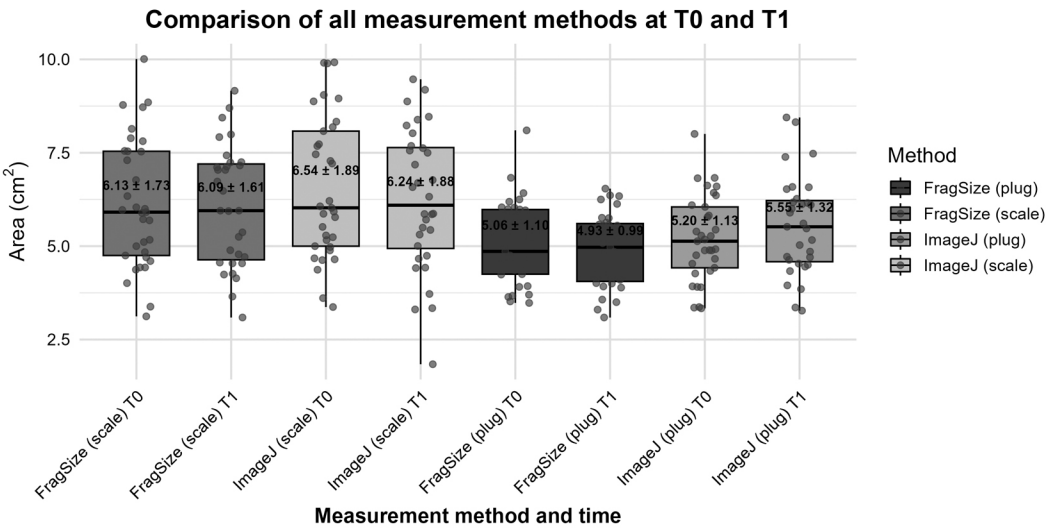

Fig. 4. Boxplots comparing fragment planar area estimates obtained using four measurement methods at T_0 and T_1. Methods included FragSize and ImageJ using either scale-based or plug-based calibration. Jittered points represent individual fragment measurements, and boxes indicate median and interquartile range; mean ± SD values are displayed for each method–time combination.

the coral fragment. This difference in distance alters the pixel-to-centimeter ratio: when the reference scale lies farther from the camera, each centimeter occupies fewer pixels, resulting in inflated area estimates. In contrast, plug-based calibration uses a reference object that lies in nearly the same optical plane as the fragment, minimizing perspective distortions and producing more stable and conservative values.

Bland-Altman: The agreement between FragSize and ImageJ was further evaluated using Bland–Altman analysis under the two equivalent calibration strategies: scale in image calibration and plug-diameter calibration (Fig. 5). In all Bland–Altman plots, the central horizontal dashed line represents the bias (mean difference between methods), while the upper and lower dashed lines indicate the 95 % limits of agreement (LoA = bias ± 1.96 SD). The Mean Absolute Percentage Error (MAPE) represents the average absolute difference between methods expressed as a percentage of the reference measurement, providing an intuitive metric of relative error magnitude.

Under scale calibration, FragSize showed strong agreement with ImageJ at both time points. In T_0, FragSize slightly underestimated ImageJ (bias = −0.41 cm²), with narrow limits of agreement (−1.51 to 0.69 cm²) and low relative error (MAPE = 6.37 %). T_1 showed a similar pattern (bias = −0.26 cm²; LoA = −1.29 to 0.78 cm²; MAPE = 7.56 %), with very high correlation (r = 0.96). These results demonstrate that scale calibration yields consistent and highly concordant measurements across both methods.

Under plug-diameter calibration, agreement also remained high. In T_0, the bias was minimal (−0.13 cm²), with moderate dispersion (SD = 0.71 cm²) and an acceptable relative error (MAPE = 10.68 %). In T_1, the bias increased moderately (−0.65 cm²), but overall agreement remained strong (MAPE = 11.15 %, r = 0.87). This indicates that FragSize reliably reproduces ImageJ measurements when both tools use the same geometric reference.

Although scale calibration produced tighter agreement between ImageJ and FragSize, this concordance does not imply higher accuracy.

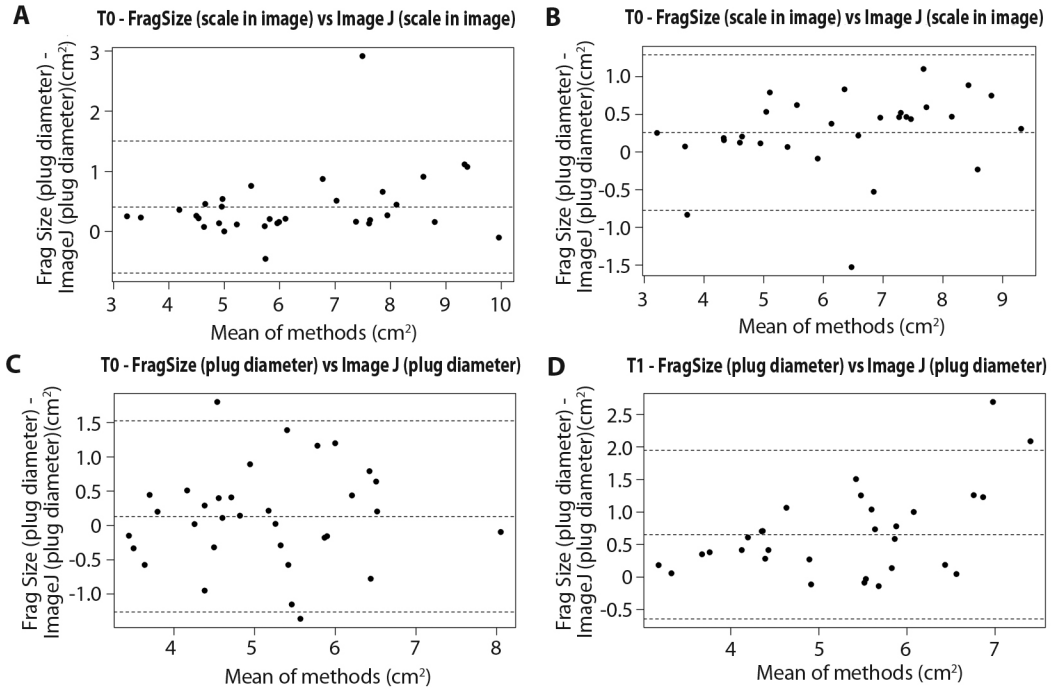

Fig. 5. Bland–Altman agreement plots comparing planar area measurements obtained with FragSize and ImageJ under matched calibration strategies. (A–B) Agreement between ImageJ and FragSize under scale calibration at T_0 (A) and T_1 (B). (C–D) Agreement under plug-diameter calibration at T_0 (C) and T_1 (D). Each plot displays three horizontal dashed lines: the middle line represents the bias, and the upper and lower lines indicate the 95 % limits of agreement (LoA). Across both calibration strategies and time points, FragSize closely reproduced ImageJ measurements, supporting its accuracy for automated planar area estimation.

Both tools rely on the same scale positioned on the acrylic table, which lies on a different optical plane than the plug and the coral fragment; consequently, both methods are similarly affected by magnification induced by perspective and therefore share the same directional bias. In contrast, plug-diameter calibration reduces this geometric distortion by placing the reference object closer to the plane of the fragment. However, the plug introduces its own sources of variability such as irregularities in diameter and differences in height that make them prone to subtle tilting which likely contributes to the higher dispersion and increased MAPE observed in plug-based comparisons. Thus, while scale calibration yields stronger agreement between methods, plug calibration remains the more reliable geometric reference despite its slightly higher error metrics.

Growth analysis by species: Species-level growth patterns were consistent across taxa. Mean fragment planar area remained relatively stable between monitoring times for *Diploria labyrinthiformis*, *Montastraea cavernosa*, and *Orbicella faveolata*. Statistical analysis results are summarized in Table 2.

Despite the absence of significant changes in planar surface area, visual inspection revealed tissue regeneration. In *Diploria labyrinthiformis*, fragments exhibited tissue recovery along the colony margin, indicating active growth not captured by two-dimensional measurements as shown in Fig. 6. Similarly, in *Montastraea cavernosa*, margin regeneration and a significant increase in polyp number were observed, further supporting the presence of biological growth independent of planar area expansion as shown in Fig. 7.

Table 2

Summary of planar area changes (mean ± SD) and statistical results by species. Mean fragment area (cm^2) was calculated separately for each genotype at each time point (T_0 and T_1).

Species	Metric	T_0 (mean ± SD, cm^2)	T_1 (mean ± SD, cm^2)	Change	p-value	Interpretation
Diploria labyrinthiformis	Planar area (range across genotypes)	4.58 ± 0.67 to 5.88 ± 1.36	3.89 ± 0.64 to 5.79 ± 0.35	Mixed but mostly stable	>0.05 (all genotypes)	No significant change
Montastraea cavernosa	Planar area (range across genotypes)	2.89 ± 0.57 to 4.49 ± 0.95	3.06 ± 0.70 to 4.85 ± 1.09	Slight increase	>0.05 (all genotypes)	Non-significant increase
Orbicella faveolata	Planar area (range across genotypes)	3.12 ± 0.57 to 3.54 ± 0.94	2.35 ± 0.55 to 4.28 ± 1.89	Mostly stable	>0.05 (most genotypes)	No significant change
Orbicella faveolata (genotype 293)	Planar area	3.12 ± 0.57	2.35 ± 0.55	Decrease	p = 0.010	Significant decrease

Values are presented as the range of genotype-level means (± SD) within each species.

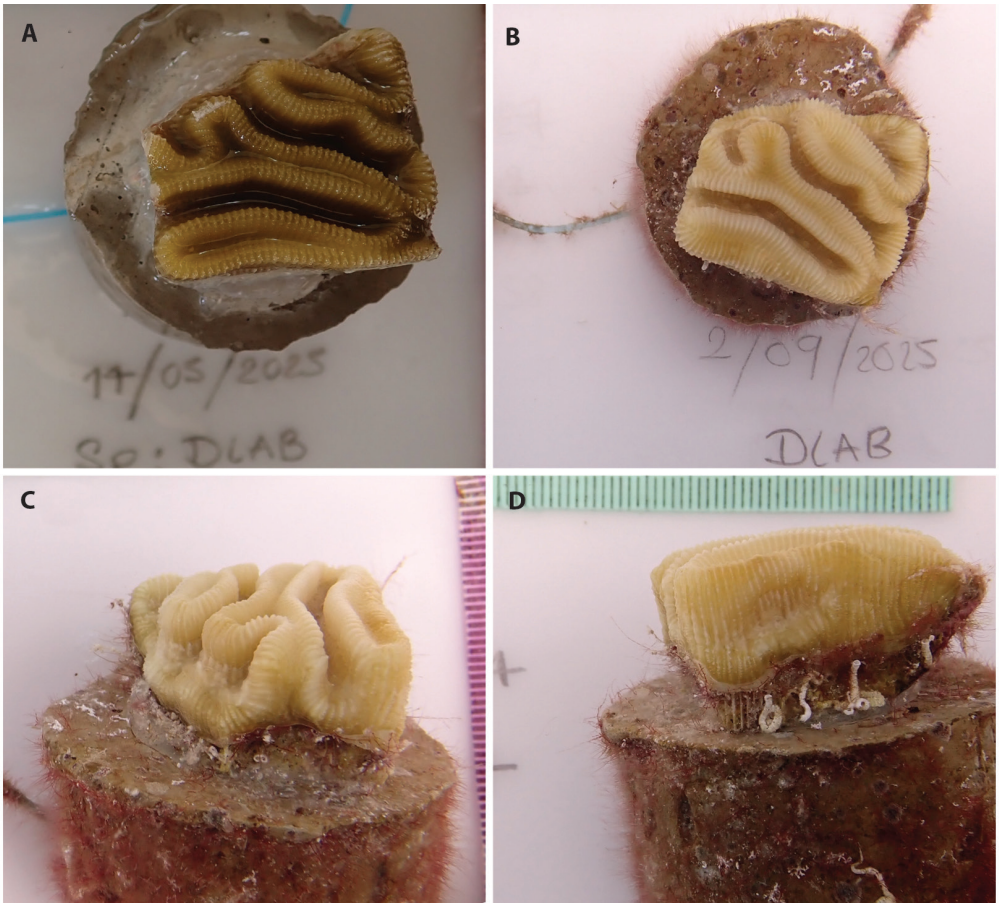

Fig. 6. Top and lateral views of *Diploria labyrinthiformis* genotype 294, fragment 67, at the beginning (T_0) and end (T_1) of the monitoring period. **A.** Top view at T_0. **B.** Top view at T_1. **C–D.** Lateral views at T_1 showing tissue coverage along the fragment margins following microfragmentation.

Revista de Biología Tropical, ISSN: 2215-2075 Vol. 74 (S1): e202610958, abril 2026 (Publicado Jul. 16, 2026)

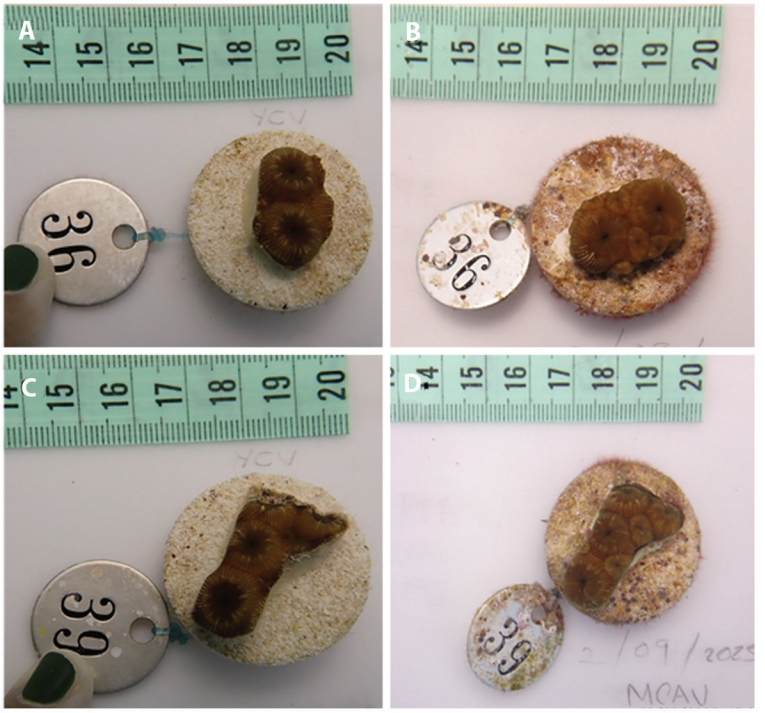

Fig. 7. Top-view photographs of *Montastraea cavernosa* genotype 300 showing two monitored fragments at the beginning (T_0) and end (T_1) of the monitoring period. (A–B) Fragment 36 at T_0 and T_1, respectively. (C–D) Fragment 39 at T_0 and T_1, respectively.

In Fig. 6 is evident that previously exposed skeletal margins generated during microfragmentation T_0 were smoother and uniformly covered by tissue, particularly along the peripheral vertical walls of the fragments at T_1 .Both *M. cavernosa* fragments showed visible colony expansion between T_0 and T_1, including the appearance of newly formed polyps along the margins of previous lesions, consistent with active peripheral tissue regeneration. Although most *Orbicella faveolata* fragments remained stable in terms of planar area, a localized decrease was observed in one genotype, associated with tissue loss. Unlike the other two species, *Orbicella faveolata* did not exhibit clear signs of margin regeneration or polyp development during the monitoring period. Instead, visual observations indicated a tendency toward deterioration at lesion edges, characterized by tissue recession and paling. These results highlight the limitations of planar measurements for capturing coral growth dynamics and emphasize the importance of complementary biological indicators and observations.

DISCUSSION

Recent advances in coral-reef monitoring increasingly incorporate computer-vision tools to automate the extraction of morphometric information from underwater images, supporting the transition toward scalable and reproducible restoration workflows. Validating such automated approaches against established manual standards is essential to ensure that new tools produce measurements that are both biologically meaningful and methodologically robust. In this study, FragSize, a YOLOv8-based segmentation tool, was evaluated by comparing its planar-area estimates with traditional

ImageJ polygon tracing under two calibration strategies. The strong correspondence between methods when operating under equivalent geometric constraints supports the suitability of FragSize for high-throughput coral monitoring.

Validation under real-world conditions: Across both T_0 and T_1, scale-calibrated measurements clustered together and differed systematically from plug-calibrated measurements, a pattern consistent with geometric constraints inherent to 2D image-based measurements. Under prospecting imaging, metric properties such as length are not preserved unless the reference and target lie within the same plane relative to the camera; differences in depth or orientation introduce changes in apparent scale and lead to systematic measurement discrepancies (Hartley & Zisserman, 2004).

In our study, the acrylic scale was positioned slightly deeper in the image than the coral fragment, which likely increased the effective pixel-to-centimeter ratio for the fragment and led to overestimation of planar area in both FragSize and ImageJ. In contrast, plug-based calibration provided a reference closer to the fragment plane, thereby reducing magnification artifacts, although minor variability due to plug tilt or irregularity may still have contributed to measurement error. The fact that both tools shifted in the same direction under each calibration strategy indicates that these discrepancies are primarily driven by imaging geometry rather than segmentation performance.

Bland–Altman analyses further demonstrated strong agreement between FragSize and ImageJ when compared under the same calibration reference. This is consistent with previous work showing that automated segmentation approaches can reproduce manual measurements when image boundaries are clearly defined and acquisition conditions are controlled (Neal et al., 2015).

Importantly, FragSize remained robust across heterogeneous photographic conditions, including variation in lighting, turbidity, and imaging medium. These factors are known to introduce noise into 2D morphometric analyses, particularly in underwater environments (Neal et al., 2015). Despite these sources of variability, FragSize produced measurements statistically equivalent to ImageJ within each calibration strategy, supporting the robustness of YOLO-based segmentation for coral monitoring applications.

Biological measurements as a proof-of-concept application: Application of FragSize to fragments of three massive Caribbean coral species demonstrated that the tool is suitable for monitoring planar area in in situ nurseries. No significant changes in planar surface area were detected between time points for any species, except for a single genotype that exhibited a significant decrease. Nevertheless, FragSize consistently captured the overall pattern of stability, while also detecting the localized decrease observed in one genotype and minor increases in others, even when these were not statistically significant. This indicates that the method is sensitive to subtle changes and reliable for tracking 2D surface dynamics under field conditions, even when growth is limited over short monitoring intervals.

Qualitative observations revealed that *Montastraea cavernosa* and *Diploria labyrinthiformis* exhibited clear signs of biological recovery, including polyp budding, tissue advancement, and marginal wound closure, which were not fully captured by planar area measurements alone. This highlights a key limitation of 2D metrics: projected planar area alone may underestimate biological recovery in corals, as early regeneration can involve tissue thickness and marginal regrowth without substantial lateral expansion (Bak & Steward-Van Es, 1980).

***Montastraea cavernosa*: Limited Planar Growth but Clear Evidence of Regeneration:** Although *M. cavernosa* fragments did not exhibit a statistically significant increase in planar surface area, they showed clear visual evidence of biological recovery. The number of visible polyps increased significantly, from a mean of 6.19 (± 2.8, SD) to 10.0 (± 3.57, SD) polyps per fragment, with an average of 3.9 (± 2.26, SD)

new polyps formed during the monitoring period. Newly formed corallite structures were visible along fragment margins and over previously exposed skeletons.

This pattern is consistent with the growth strategy of massive corals, in which early recovery following fragmentation may involve tissue repair and polyp proliferation before measurable horizontal expansion (Bautista, 2024; Knapp et al., 2022). These findings suggest that planar surface area alone underestimates regeneration in *M. cavernosa* over short timescales, and that polyp production may serve as a more sensitive indicator of early recovery.

Diploria labyrinthiformis: **visible wound closure but minimal 2D expansion*:*** *Diploria labyrinthiformis* fragments showed negligible changes in planar area; however, profile observations revealed consistent tissue regrowth along margins and partial coverage of exposed skeleton. These findings indicate active healing despite the absence of detectable changes in top-down area measurements.

This discrepancy reflects known limitations of planar measurements for dome-shaped and massive corals. Early recovery in these species may involve vertical growth and tissue thickening rather than lateral expansion, processes that are not captured in 2D projections (Neal et al., 2015) specially in very short periods of time. Consequently, planar measurements alone may underestimate recovery dynamics in such morphologies.

***Orbicella faveolata*: Low Regeneration During Early Recovery:** *Orbicella faveolata* exhibited limited biological activity during the study period. Planar surface area remained stable across genotypes, and no significant increase in polyp number was observed. One genotype displayed localized tissue loss, consistent with patterns of early-stage stress and tissue retraction reported in small fragments of this species (Bautista, 2024).

Previous studies have shown that *Orbicella faveolata* exhibits relatively slow growth rates and a limited response to fragmentation compared to other massive corals, even under controlled conditions (Steinberg, 2021). In in situ environments, this response may be further constrained by environmental stressors such as algal competition and sedimentation, which can offset early gains in tissue coverage (Bautista, 2024).

Taken together, these findings suggest that *Orbicella faveolata* may require longer recovery periods, more favorable environmental conditions, or bigger fragment size for in-situ nursery rearing. The stability observed in this study likely reflects a conservative growth strategy and lower apparent regeneration rates during early recovery stages.

Environmental context and interpretation of limited planar growth: The absence of measurable 2D expansion should not be interpreted as a failure of FragSize to detect growth. Instead, it likely reflects environmental constraints intrinsic to in situ nurseries. Factors such as algal overgrowth, sediment accumulation, hydrodynamic stress, unequal and short nursery residence times may have limited detectable planar expansion during the monitoring interval. Under these conditions, FragSize correctly identified the overall pattern of planar stability, while complementary qualitative observations revealed ongoing biological healing, supporting its suitability for monitoring changes in planar area.

Limitations and future directions: This study highlights several considerations for future applications of FragSize. The monitoring interval was short relative to typical restoration timescales, which limited our ability to detect longer-term growth trajectories. However, this timeframe was still informative, as it allowed the detection of important features of the early recovery phase, including patterns of planar stability, localized tissue loss, and qualitative signs of regeneration that would have been overlooked without repeated monitoring. Extending the monitoring period would strengthen the interpretation of genotype-specific growth trajectories and longer-term performance. In

parallel, continued expansion of the training dataset with annotated images should further improve model robustness and generalizability. This also opens the possibility of generating larger longitudinal datasets, enabling higher-throughput monitoring and longer-term tracking of individual genotypes in restoration settings. Because planar measurements capture projected area only, future applications would also benefit from combining FragSize with complementary approaches such as lateral imaging or 3D photogrammetry to provide a more complete representation of colony recovery.

Our findings support the use of FragSize as a scalable and reproducible tool for coral restoration monitoring. While planar area remained largely stable during the study period, this stability reflects early-stage biological responses in in situ conditions rather than methodological insensitivity. By accurately capturing these stable trends, FragSize provides a reliable quantitative tool that can be complemented with visual assessments of wound healing and polyp number. As restoration programs expand and require early detection of disease lesions or long-term fragment monitoring, automated tools such as FragSize will be essential for increasing sample sizes, reducing observer bias, and harmonizing monitoring protocols across sites and institutions. In the future, integrating this planar morphometrics obtained with FragSize with qualitative and potentially 3D assessments will allow restoration practitioners to more fully capture species-specific recovery trajectories while maintaining the efficiency and standardization needed for large-scale implementation.

Ethical statement: The authors declare that they all agree with this publication and made significant contributions; that there is no conflict of interest of any kind; and that we followed all pertinent ethical and legal procedures and requirements. All financial sources are fully and clearly stated in the acknowledgments section. A signed document has been filed in the journal archives.

ACKNOWLEDGMENTS

We would like to sincerely thank all the individuals who contributed to this study through their assistance with fieldwork, data collection, coral monitoring, and technical support. Their dedication and commitment were fundamental to the successful completion of this research. We are especially grateful to Fundación Blue Indigo´s team who helped us clean and monitor our coral nurseries. We also thank the Corporación para el Desarrollo Sostenible del Archipiélago de San Andrés, Providencia y Santa Catalina (CORALINA) and for their valuable collaboration, expertise, and logistical support. Their contributions greatly facilitated the development of this research and strengthened its scientific scope. Finally, we thank our colleagues and reviewers for their help through this process.

REFERENCES

Aronson, R. B., & Precht, W. F. (2001). White-band disease and the changing face of Caribbean coral reefs. *Hydrobiologia*, *460*, 25–38. https://doi.org/10.1023/A:1013103928980

Bak, R. P., & Steward-Van Es, Y. (1980). Regeneration of superficial damage in the scleractinian corals *Agaricia agaricites* f. *purpurea* and *Porites astreoides*. *Bulletin of Marine Science*, *30*(4), 883–887.

Bautista, T. (2024). *Maximizing coral tissue production: The role of fragment size and grow- out location* [Master's thesis]. University of Miami, United States of America. https://scholarship.miami.edu/esploro/outputs/graduate/Maximizing-Coral-Tissue-Production-The-Role/991032486168902976

Bradski, G. (2000). The opencv library. *Dr. Dobb's Journal: Software Tools for the Professional Programmer*, *25*(11), 120–123.

Cramer, K. L., Jackson, J. B. C., Donovan, M. K., Greenstein, B. J., Korpanty, C. A., Cook, G. M., & Pandolfi, J. M. (2020). Widespread loss of Caribbean acroporid corals was underway before coral bleaching and disease outbreaks. *Science Advances*, *6*(17), eaax9395. https://doi.org/10.1126/sciadv.aax9395

Dwyer, B., Nelson, J., Hansen, T., & Roboflow Inc. (2025). Roboflow (Version 1.0) [Software]. https://roboflow.com

Forsman, Z. H., Page, C. A., Toonen, R. J., & Vaughan, D. (2015). Growing coral larger and faster: micro-colony-fusion as a strategy for accelerating coral cover. *PeerJ*, *3*, e1313. https://doi.org/10.7717/peerj.1313

Frias-Torres, S., Reveret, C., Henri, K., Shah, N., & Montoya Maya, P. H. (2023). A low-tech method for monitoring survival and growth of coral transplants at a boutique restoration site. *PeerJ*, *11*, e15062. https://doi.org/10.7717/peerj.15062

Gladfelter, W. B. (1982). White-band disease in Acropora palmata:implications for the structure and growth of shallow reefs. *Bulletin of Marine Science*, *32*(2), 639–643.

Green, E. P., & Bruckner, A. W. (2000). The significance of coral disease epizootiology for coral reef conservation. *Biological Conservation*, *96*(3), 347–361. https://doi.org/10.1016/S0006-3207(00)00073-2

Hartley, R., & Zisserman, A. (2003). *Multiple view geometry in computer vision*. (2nd ed) Cambridge University Press.

Jocher, G., Qiu, J., & Chaurasia, A. (2023). *Ultralytics YOLO* (Version 8.0.0) [Computer software]. https://github.com/ultralytics/ultralytics

Knapp, I. S. S., Forsman, Z. H., Greene, A., Johnston, E. C., Bardin, C. E., Chan, N., Wolke, C., Gulko, D., & Toonen, R. J. (2022). Coral micro-fragmentation assays for optimizing active reef restoration efforts. *PeerJ*, *10*, e13653. https://doi.org/10.7717/peerj.13653

Lirman, D., Schopmeyer, S., Galvan, V., Drury, C., Baker, A. C., & Baums, I. B. (2014). Growth dynamics of the threatened Caribbean Staghorn Coral *Acropora cervicornis*: influence of host genotype, symbiont identity, colony size, and environmental setting. *PLoS One*, *9*(9), e107253. https://doi.org/10.1371/journal.pone.0107253

Neal, B. P., Lin, T. H., Winter, R. N., Treibitz, T., Beijbom, O., Kriegman, D., Kline, D. I., & Greg Mitchell, B. (2015). Methods and measurement variance for field estimations of coral colony planar area using underwater photographs and semi-automated image segmentation. *Environmental Monitoring and Assessment*, *187*(8), 496. https://doi.org/10.1007/s10661-015-4690-4

OpenAI. (2025). *ChatGPT and Codex language models* [Large language models]. https://openai.com

Page, C. A., Muller, E. M., & Vaughan, D. E. (2018). Microfragmenting for the successful restoration of slow growing massive corals. *Ecological Engineering*, *123*, 86–94. https://doi.org/10.1016/j.ecoleng.2018.08.017

Papke, E., Carreiro, A., Dennison, C., Deutsch, J. M., Isma, L. M., Meiling, S. S., Rossin, A. M., Baker, A. C., Brandt, M. E., Garg, N., Holstein, D. M., Traylor-Knowles, N., Voss, J. D., & Ushijima, B. (2024). Stony coral tissue loss disease: a review of emergence, impacts, etiology, diagnostics, and intervention. *Frontiers in Marine Science*, *10*, 1321271. https://doi.org/10.3389/fmars.2023.1321271

Python Software Foundation. (2023). *Python (Version 3.11)* [Computer software]. https://www.python.org

Roff, G. (2021). Evolutionary history drives biogeographic patterns of coral reef resilience. *BioScience*, *71*(1), 26–39. https://doi.org/10.1093/biosci/biaa145

R Core Team. (2022). *R: A language and environment for statistical computing*. R Foundation for Statistical Computing. https://www.R-project.org/

RStudio Team. (2022). *RStudio: Integrated development environment for R*. RStudio, PBC. https://www.rstudio.com/

Santodomingo, N., Flórez, P., & Reyes, J. (2010). *Corales escleractinios de Colombia*. Instituto de Investigaciones Marinas y Costeras (INVEMAR).

Steinberg, A. A. (2021). Optimization of grow-out of bouldering coral microfragments: land vs. offshore nursery [Master's thesis]. Nova Southeastern University, United States of America. https://nsuworks.nova.edu/hcas_etd_all/44